Effects of needleleaf forest cover on radiation and snowmelt dynamics in the Canadian Rocky Mountains

Ellis, CR, Pomeroy, JW, Essery, RLH & Link, TE 2011, 'Effects of needleleaf forest cover on radiation and snowmelt dynamics in the Canadian Rocky Mountains' *Canadian journal of forest research-revue canadienne de recherche forestiere*, vol 41, no. 3, pp. 608-620.

Effects of Needleleaf Forest Cover on Radiation and Snowmelt Dynamics in the Canadian Rocky Mountains

C.R. Ellis, J.W. Pomeroy, R.L.H. Essery, T. E. Link

C. R. Ellis. Centre for Hydrology, Department of Geography, University of Saskatchewan, Canada.

J. W. Pomeroy. Centre for Hydrology, Department of Geography, University of Saskatchewan, Canada.

R. L. H. Essery. School of Geosciences, University of Edinburgh, Edinburgh, U.K.,

T. E. Link. Department of Forest Resources, University of Idaho, Moscow, USA.

Abstract

Utilizing extensive field observations, the effect of needleleaf forest cover on radiation and snowmelt timing was quantified at pine and spruce forest sites and nearby clearings of varying slope and aspect in an eastern Canadian Rocky Mountain headwater basin. Compared to open clearing sites, shortwave radiation was much reduced under forest cover, resulting in smaller differences in melt timing between forested slopes relative to open slopes with different aspects. In contrast, longwave radiation to snow was substantially enhanced under forest cover, especially at the dense spruce forest sites where longwave radiation dominated total energy for snowmelt. In both pine and spruce environments, forest cover acted to substantially reduce total radiation to snow and delay snowmelt timing on south-facing slopes, while increasing total radiation and advancing snowmelt timing on north-facing slopes. However, forest cover effects were less pronounced on level terrain, where radiation and the rate of snowmelt was slightly less under forest cover compared to that in the open. Results strongly suggest that impacts on radiation to snow and snowmelt timing from changes in mountain forest cover will depend much on the slope and aspect at which changes occur.

Introduction

Snowmelt is one of the most important hydrological events in mountain regions, responsible for soil moisture recharge (e.g. Grant et al., 2004), vegetation growth (e.g. Cooper et al., 2006) and ecosystem productivity (e.g. Arp et al., 2006). Mountain snowmelt is the source of the majority of river flows in western North America (Marks and Winstral, 2001) and are hence of great importance to downstream water resource users. As much of North American cold regions mountain terrain is covered by evergreen needleleaf forest, turbulent energy exchanges to sub-canopy snowcovers are suppressed (Harding and Pomeroy, 1996) and snowmelt is driven primarily by radiation (United States Army Corps of Engineers, 1956). This is with exception of more coastal mountain environments where large amounts of snowmelt energy may be delivered through rainfall, having the potential to cause rapid melt and flooding (Beaudry and Golding, 1983; Marks et al., 1998). However, for more interior mountain ranges, effective prediction of the timing and magnitude of snowmelt runoff is expected to require an understanding of how needleleaf forest cover influences radiation for snowmelt across complex terrain. Extensive field studies by Golding and Swanson (1978) and Troendle and Leaf (1981) have shown the timing and rate of snowmelt to differ substantially between level forests and clearings. Yet comparatively little has been reported regarding the combined effects of forest cover and slope and aspect on snowmelt in mountain regions. Together, information of both forest cover and topography effects are expected to be important in anticipating how the changes in forest cover (e.g. clearcutting, fire, disease) may impact the timing of snowmelt in mountain regions (Gary, 1980).

Quantification of net all-wave radiation to snow (R^*) is made by the sum of net shortwave (K^*) and net longwave (L^*) balances, each composed of incoming and outgoing fluxes, i.e.

[1] $$R^* = K^* + L^* = K_{in} - K_{out} + L_{in} - L_{out}$$

Here, K^* is related to K_{in} by the snow albedo (α_s) through

[2] $$K^* = K_{in} - K_{out} = K_{in}(1 - \alpha_s)$$

Forest cover has been observed to have a counteracting effect on radiation to snow by reducing shortwave irradiance via canopy extinction (i.e. reflection and absorption) (Ellis and Pomeroy, 2007; Link and Marks, 1999) while increasing longwave irradiance from foliage thermal emissions (Black et al., 1991; Reifsnyder and Lull, 1965). Here, the reduction of shortwave irradiance in forests is commonly expressed in terms of the forest shortwave transmittance (τ):

[3] $$\tau = \frac{K_{in}}{K_o}$$

where K_{in} and K_o denote the sub-canopy and above-canopy shortwave irradiance fluxes, respectively. The offsetting of shortwave reductions in forests by canopy longwave emissions is promoted particularly during conditions of high snow albedo (Jeffrey, 1970), and in high latitudes or altitude environments where atmospheric longwave emissions are relatively low (Sicart et al., 2004).

Although much focus has been placed on quantifying radiation for snowmelt in level needleleaf forests (e.g. Gryning and Batchvarova 2001; Metcalfe and Buttle, 1995), how variations in topography (i.e. slope and aspect) and forest cover control radiation to snow in mountain systems is comparatively lacking in the literature. Such information would improve the understanding of how radiation to snow

varies across complex terrain and help identify needs for future developments of spatially distributed snowmelt models (e.g. Marks et al., 1999).

The primary objective of this study is to quantify the effects of both forest cover and slope and aspect on radiation to snow and the timing of snowmelt in mountain environments. Particular focus will be placed on examining how topography and forest cover determine the relative amounts of shortwave and longwave radiation to snow, as well as their contributions to snowmelt energy in both lower elevation pine forest stands and higher elevation spruce forest stands. This will be accomplished through analysis of radiation and other field meteorological observations, as well as snow survey data collected at paired forest and clearing sites of varying elevation, slope and aspect located in a headwater basin in the eastern slopes of the Canadian Rocky Mountains. Although analysis relies primarily upon field observations, appropriate corrections and estimations of radiation fluxes and meteorological variables are made where necessary.

Observation sites and instrumentation

Observation sites

All field observations were made at the Marmot Creek Research Basin (MCRB), Alberta, Canada (50°57`N, 115°09`W) (Figure 1). Elevation of the basin ranges from 1550 to 2750 m.a.s.l. with the lower elevations covered by lodgepole pine forest (*Pinus contorta* var. Latifolia) and upper elevations by Engelmann spruce (*Picea engelmannii*), subalpine fir (*Abies lasiocarpa*) and alpine larch (*Larix lyallii*). During the spring of 2005, near-surface meteorological observations were made at the following sites: a level pine clearing (LPC), a level pine forest (LPF), a north-facing pine forest (NPF), a southeast-facing pine clearing (SPC), and a southeast-facing pine forest (SPF). Similar observations were made during the spring of 2008 at a level spruce clearing (LSC), a north-facing spruce forest (NSF) and a

south-facing spruce forest sites (SSF). Snow surveys were conducted at all pine and spruce sites during their respective study periods, as well as at north-facing spruce clearing (NSC) and south-facing spruce clearing (SSC) sites located adjacent to the NSF and SSF sites, respectively. To allow a greater comparison of radiation and snowmelt between sloping clearing and forest sites, simulations of shortwave irradiance were made to a hypothetical north-facing pine clearing (NPC) of the same slope and aspect as the NPF site, as well to the non-instrumented NSC and SSC sites using standard radiation correction procedures for topography. The locations of all study sites at the MCRB are shown in Figure 1, with descriptions of the topography and forest cover at each site provided in Table 1. Analysis of both the 2005 pine and 2008 spruce meteorological and snow survey datasets focuses on two primary observation periods: (i) an extended observation period spanning from February 15 to May 15 at both pine and spruce sites, allowing the comparison of meteorological conditions over the same springtime period, and (ii) the period during snowpack warming and melt, extending from March 13 to April 4, 2005 (DOY 72 to 95) at the pine sites, and from March 30 to May 29, 2008 (DOY 90 to 150) at the spruce sites. Reference meteorological conditions observed at the LPC and LSC during the respective extended February to May observation periods as well as the snowpack warming and melt periods are given in Table 2.

Table 1 inserted here

Table 2 inserted here

Figure 1 inserted here

Instrumentation

Radiation sensors

Radiometers at the meteorological observation sites were positioned approximately 1.5 m above the snow surface and inclined parallel to their respective ground surfaces; thus radiation fluxes always refer to the direction normal to the ground surface. Incoming and outgoing shortwave and longwave fluxes were measured respectively using recently calibrated Kipp and Zonen pyranometers and pyrgeometers (radiometer manufacturer specifications are provided in Table 3). Radiometers were controlled and measurements stored by Campbell Scientific dataloggers (23X, 10X) with observations acquired every 10 s and time-averaged values stored at 15 min intervals. Shortwave and longwave fluxes at each site were measured by single radiometers, with the exception of the southeast-sloping pine forest (SPF) where two additional upward-facing pyranometers and pyrgeometers were deployed to better account for the increased spatial variation of forest cover.

Table 3 inserted here

Accurate measurements of radiation in the field are challenging due to both instrument and sampling errors, each of which may be random or systematic in nature (Moore and Rowland, 1990). However, with the use of recently calibrated radiometers at all study sites, systematic instrument errors were considered solely random and are specified according to the manufacturer in Table 3. In forests, the accurate measurement of incoming radiation (i.e. irradiance) is further complicated due to the heterogeneous spatial distribution of canopy cover (Link et al. 2004; Pomeroy et al., 2008), which among the forest study sites was most pronounced at the LPF and SPF. To account for potential sampling errors at these sites, shortwave and longwave irradiance from the permanent *site* radiometers were corrected to that measured by an *array* of 10 pyranometers and 12 pyrgeometers at each site. The single *array* radiometers were spatially positioned randomly near the permanent *site* radiometers at

the LPF and SPF sites, being located at varying proximity to forest trunks. Observations of daily shortwave and longwave irradiance (both abbreviated here as I_{in}) from the permanent *site* radiometers (obs.) were corrected (corr.) to that of the *array* by the mean bias (*MB*) coefficient between the two, i.e.

$$\begin{aligned} \text{corr. daily } site\ I_{in} &= (\text{obs. daily } site\ I_{in})\ MB \\ &= (\text{obs. daily } site\ I_{in})\ \frac{\sum_{t=0}^{t=n} I_{in}\ (array)}{\sum_{t=0}^{t=n} I_{in}\ (site)} \end{aligned} \quad [4]$$

where t=0 to t=n define the start and end of the time period of *array* observations. Differences in irradiance between the permanent site observations and array observations at the LPF and SPF are stated both in terms of absolute magnitudes and *MB* in Table 4. Although uncertainty exists in how representative *MB* values are over the extended observation period due to effects such as changing solar elevations, resulting errors are likely small considering the small changes in shortwave and longwave spatial variation in these forests over daily time scales or longer (Pomeroy et al., 2008; Essery et al., 2008). This is further supported by the MB values calculated over hourly time scales at both sites, which with the exception of early morning and late evening periods, compared well to daily values.

Table 4 inserted here

Temperature sensors

Snow and canopy foliage temperatures were measured every 10 s with average values recorded and stored at 15 min intervals during the respective study periods at the meteorological observation

sites, as were the south-exposed trunk surface temperatures at the LPF, SPF, NSF and SSF. Temperatures were measured using Exergen IRt/c.5-K-50F/10C (capacitor removed) infrared thermocouples (IRt/c), having an expected error to that of true temperature ranging from ±0.01 °C at 0 °C, to ±2 °C at 24 °C (Omega IRt/c operator's manual, 1994), and which were housed within reflective enclosures to minimize errors from shortwave heating. Air temperatures were measured approximately 2 m above the ground surface at all sites using Vaisala HMP45A combination temperature/humidity sensors housed within Gill radiation shields, having an expected error of ±0.1°C (Vaisala technical manual, 2008).

Description of forest cover density

At all study sites, upward-looking hemispherical images were obtained at positions corresponding to each of the permanent *site* radiometers and *array* radiometers during overcast sky conditions for the purpose of digital analysis. Images were acquired using a Nikon Coolpix 5000 digital camera fitted with a 183° field of view fisheye converter lens. Estimates of the effective leaf-area index (*LAI*`), defined here as being equal to one-half of the total plant surface area not self-shaded by foliage clumping effects per unit ground surface area, were made at the LPF, NPF, SPF, SPC, NSF, SSF from hemispherical image analysis using GLA 2.0 software (Frazer et al., 2000). This software computes the angular distribution of gap and non-gap fractions of a hemispherical forest scene by the division of image pixels into 'sky' and 'non-sky' classes. Alternatively, the sky view factor (*v*) of each forest site was approximated as the measured shortwave transmittance (at the LPF and SPF mean *array* irradiance was used for this purpose) during cloud covered days when radiation variations across the sky hemisphere are relatively small. At the LPC and LSC, where surrounding terrain occupied the sky view, *v* was estimated from analysis of digital elevation data of the MCRB and surrounding area.

Snow surveys

Measurements of snow water equivalent (SWE) were obtained from surveys of snow depth and density repeated approximately every 2 to 3 weeks prior to snowmelt and every 2 to 3 days during snowmelt. Snow depth measurement were performed along established transects at a spacing of approximately 1 m at the clearing sites, and a spacing of about 0.5 m at the forest sites to account for the greater spatial variation of forest snow depth. Determinations of snow density were made from snow mass measurements taken at every 5^{th} depth sample using either an ESC-30 snow tube (and calibrated scale), or a Perla-style (RIP) snow cutter scoop in which samples taken along the vertical profile of a dug snowpit and weighed in the field using an electronic balance. At the meteorological observation sites, the relating of snow survey areal depths to continuous point depth measurements acquired by a SR50 sonic ranger allowed the construction of continuous and spatially representative dataset of snow depth and SWE for each site.

Results

Shortwave irradiance (K_{in})

Over the extended February to May period at both the pine and spruce locations, mean daily shortwave irradiance (K_{in}) between sites varied substantially, ranging from approximately 1.5 MJ m^{-2} at the north-facing forests (NPF and NSF sites), to greater than 15 MJ m^{-2} at the south-facing clearings (SPC and SSC sites); equal to a ratio of approximately 0.1 and 1.2 to that observed at their respective level clearings (LPC and LSC sites) (Table 5). Overall, forest cover acted to greatly reduce the absolute differences in K_{in} produced by slope and aspect effects, especially between the spruce forest sites where the low forest shortwave transmittances (τ) of 0.12 at the NSF and 0.11 at the SSF gave corresponding low daily K_{in}

daily values of 1.5 and 1.7 MJ m^{-2}. By comparison, shortwave transmittances exhibited much greater variation among the pine forest sites, with mean τ values ranging from 0.34 at the SPF to 0.13 at the NPF, producing corresponding daily K_{in} magnitudes of 5.4 and 1.4 MJ m^{-2} (Table 5).

In the pine forest, the high shortwave transmittance (τ) through the SPF resulted in a pronounced increase in the ratio of daily sub-canopy K_{in} to above-canopy K_{in}, with decreased ratios at the lower transmittance LPF and NPF sites. Consequently, differences in sub-canopy K_{in} between the pine forest sites increase progressively as above-canopy K_{in} increases, as observed at the LPC site (Figure 2). By contrast, the low τ through spruce forest results in little response in sub-canopy K_{in} at either the north-facing NSF site or the south-facing SSF site to changes in above-canopy K_{in} observed at the level spruce clearing (LSC) site (Figure 3). As a result, similar low magnitudes of sub-canopy K_{in} are maintained at both the NSF and SSF sites regardless of changing above-canopy K_{in}.

Table 5 inserted here

Figure 2 inserted here

Figure 3 inserted here

Longwave irradiance (L_{in})

As a result of canopy longwave radiation emissions, longwave irradiance (L_{in}) to snow at the forested sites was much greater than at the clearing sites over the February to May period (Table 6). Note here that as no observations of L_{in} were made at the sloped clearing sites, values at these sites were assigned the same as their respective level clearing sites (i.e. LPC, LSC), as substantial differences of L_{in} in the open are expected only from variations in longwave emissions from surrounding terrain during clear sky conditions (Sicart et al., 2004). As shown in Table 6, despite a lower overall L_{in} at the spruce forest sites relative to the pine

forests, the amount of sub-canopy longwave enhancement was similar among both the pine and spruce forests. At the spruce forest sites, sub-canopy longwave enhancements are attributed primarily to increased forest longwave emissions from the dense canopy coverage. Alternatively, at the sparser pine sites, sub-canopy longwave enhancements are also ascribed to added longwave emissions from canopy heating via shortwave irradiance absorption (Pomeroy et al., 2009). Such heating is most marked at the SPF site, where the sparse canopy coverage and more southern orientation of the site allow increased penetration of shortwave irradiance and heating of the lower trunk layer of the canopy. Such heating may be substantial, as observed by south-exposed trunks temperatures being more than 20 ˚C warmer than air temperatures during midday periods of high shortwave irradiance. Similar shortwave canopy heating effects on sub-canopy longwave irradiance have been investigated and reported by Pomeroy et al. (2009) in various needleleaf forest stands. Alternatively, no substantial longwave enhancement from canopy shortwave heating was observed at either of the spruce forest sites, which is attributed to the extinction of shortwave irradiance higher within the dense canopies at these sites.

Table 6 inserted here

Net shortwave radiation (K)*

At sites at which both incoming and outgoing shortwave fluxes were observed, net shortwave radiation (K^*) to snow was determined via Eq. 2. However, in forest environments, acccurate determinations of K^* to snow using K_{out} observations are subject to error from the exposure of dark understory vegetation as snowcover ablates. To minimize such errors, K_{out} observations were used in determining K^* only during times of complete snowcover within the field of view of the downward-facing radiometer as determined from daily field notes and photographs of snowcover at each site

during melt. For periods of partial snowcover, K^* was instead estimated through a linear extrapolation of the daily snow albedo (α_s) decay rates determined during continous snowcover. Although this method is unlikely to provide an exact representation of the many factors governing snow albedo decay rates at each site, it does provide a general approximation of K^* for the purpose of further analysis.

At the NPC, α_s was approximated by values observed at the LPC. However, at the NSC and SSC sites, where α_s observations from a nearby clearing were not available, daily α_s was instead estimated by regression relations developed between daily forest α_s values from radiometer measurements and α_s at the corresponding clearing site determined from reflectance measurements obtained using a portable spectrophotometer (Analytical Spectral Devices FieldSpec-FR). Spectrophotometer reflectance measurements were made at the NSC and SSC approximately every 48 hours for a period of 10 days prior to and after the onset of melt (i.e. DOY 130) following the procedure outlined by Melloh et al. (2001), in which 50 spectrophotometer measurements were obtained at each site to reduce random sampling errors and to minimize the ratio of noise-to-signal returns. To account for the effects of varying angular reflectance from snow, measurements were obtained over a large range of angles to the snow surface. Best approximation of clearing α_s from forest α_s values were made via separate linear regression relations for the periods of pre-melt and melt (i.e. melt occurring at one or both sites), with strongest relations between clearing and forest sites on both slopes obtained for the pre-melt period (i.e. $R^2 = 0.90$ (NSC-NSF); $R^2 = 0.97$ (SSC-SSF)). By comparison, the slightly weaker relations during the melt period ($R^2 = 0.72$ (NSC-NSF); $R^2 = 0.73$ (SSC-SSF)) resulted from the divergence in snow albedo decay rates for melting and non-melting snow between the paired clearing and forest sites. To maintain a realistic representation of snow albedo, estimated α_s values were constrained to a minimum of 0.6, which closely corresponds to the lower limit of values obtained from

spectrophotometer measurements over unlittered snow. Lastly, upon the complete disappearance of snowcover, α_s was set to 0.2 to approximate bare ground albedo.

Net longwave radiation (L)*

Similar to that of reflected shortwave irradiance, no direct observations of longwave exitance from snow (L_{out}) were obtained at the NPC, NSC, and SSC sites. Instead, L_{out} was estimated from snow surface temperatures (T_s) at these sites using the following the longwave-psychrometric formulation by Pomeroy and Essery (2010)

[5] $$T_s = T_a + \frac{\varepsilon_s(L_{in} - \sigma T_a^4) + \lambda_s(\omega_a - \omega_s)\rho_a/r_a}{4\varepsilon_s\sigma T_a^3 + (c_p + \lambda_s\Delta)\rho_a/r_a}$$

where ε_s is the thermal emissivity of snow [0.98] (Oke, 1987), σ is the Stephan-Boltzmann constant [5.67 x 10^{-8} W m^{-2} K^{-4}], ω_a and ω_s are the respective specific and saturation mixing ratios [dimensionless], c_p is the specific heat capacity of air [MJ kg^{-1} K^{-1}], ρ_a is the density of air [kg m^{-3}], λ_s is the latent heat of sublimation for ice [MJ kg^{-1}], r_a is the aerodynamic resistance [s m^{-1}], and Δ is the slope of the saturation vapour pressure curve [kPa K^{-1}]. Estimates of T_s by Eq. 5 were made using T_a observations from the paired forest sites, as well as wind speeds which were adjusted to account for forest sheltering effects in proportion to forest cover density (Ellis et al., 2010). Comparison of simulated T_s with those observations at the LPC over a two week period in shows good estimation using the approach, with mean observed and simulated T_s values for the period equal to -13.7 °C and -12.5 °C, respectively, which were both substantially colder than the mean air temperature of -8.1 °C over the period.

From simulations of T_s, the net longwave radiation (L*) at each site was resolved as the balance of incoming longwave irradiance to snow and longwave exitance from snow by

[6] $$L^* = \varepsilon_s (L_{in} - \sigma T_s^{\,4})$$

Net radiation and ablation rates during periods of snowpack warming and melt

Time series data of snow water equivalent (SWE) as well as magnitudes of daily net shortwave (K^*) and daily net longwave radiation (L^*) are shown over the respective periods of snowpack warming and melt at the pine sites (2005) in Figure 4, and at the spruce sites (2008) in Figure 5. Here, the comparison between pine and spruce sites reveals a marked difference in snow accumulations, with those at the higher elevation spruce location approaching roughly 5 fold the accumulations at the lower elevation pine sites. Although it must be noted that this comparison is made between observations from different years, snow survey data from other years indicate that these amounts largely typify snow accumulations at these locations, both in absolute terms and in the relative amounts between sites. Large differences in snow accumulations are also seen between that in the open and under forest cover, with interception losses ranging from about 40-60 % in both pine and spruce forests.

In general, the effect of forest cover on snowmelt timing differs substantially with slope and aspect. On south-facing aspects, the start of snowmelt was delayed under forest cover relative to in the open by approximately 8 days at the pine locations (Figure 4a) and 15 days at the spruce locations (Figure 5a). On level topography, observations at the pine sites show snowmelt beginning at both the LPC and LPF on DOY 85, with slightly more rapid snow melt at the clearing site. Similarly, snowmelt began on DOY 130 at both the north-facing spruce clearing (NSC) and spruce forest (NSF) sites, but with much slower melt at the clearing site where a substantial snowpack remained until the end of the observation period.

In addition to melt rate differences between paired forest and clearing sites, overall slower snowmelt rates were observed at the pine sites relative to the spruce sites. Here, mean daily melt rates ranged from 4.6 to 1.6 mm SWE d^{-1} at the pine SPC and NPF sites, respectively, compared to more rapid melt rates ranging from 12.9 to 5.4 mm SWE d^{-1} at the spruce SSC and NSC sites. Note that there were no snow data from the hypothetical NPC site for the purpose of snowmelt rate comparison. Among the pine forest sites alone, considerable differences in melt rates were also observed, equal to 3.7, 2.8 and 1.6 mm SWE d^{-1} at the SPF, LPF, NPF, respectively. In comparison, much higher melt rates were observed in the spruce forests, but with little difference between north-sloping and south-sloping sites, with corresponding melt rates of 11.3 and 11.1 mm SWE d^{-1} at the NSF and SSF.

Over the period of snowpack warming and melt, Figures 5 and 6 show radiation at all pine and spruce clearing sites to be largely dominated by net shortwave, as net longwave (L^*) was strongly negative. Longwave losses were especially pronounced at the pine clearing sites, where mean L^* losses exceeded 3 MJ m^{-2} d^{-1}, as compared to the more modest longwave losses of less than 2 MJ m^{-2} d^{-1} at the spruce clearing sites. Alternatively, much smaller K^* and L^* balances were realized at all forest sites, with slight negative and positive L^* balances among the pine forest sites; but substantial L^* gains at the spruce forests, which dominated total radiation to snow. Longwave gains to snow at the spruce forest sites were most pronounced during snowmelt events (i.e. periods starting DOY 104, 118, and 130) when air and canopy temperatures were above-freezing and longwave exitance (L_{out}) was limited by the restriction of snow surface temperature (T_s) to a maximum of 0°C. A summary of the mean daily net radiation terms during the main snowmelt event at the pine sites (starting on DOY 84) and the main snowmelt event at the spruce sites (staring on DOY 130) is

shown in Figure 6. At each site, radiation terms are shown compared to the mean amount of energy consumed by melt (Q_m) [MJ m^{-2} d^{-1}] as determined from the mean snowmelt rate (M) [kg m^{-2} d^{-1}] by

[7] $$Q_m = \beta \lambda_f M$$

where β is the fraction of ice in wet snow, which was specified in Eq. 7 equal to 0.96, and λ_f is the latent heat of fusion for ice [MJ kg^{-1}]. Overall, Figure 6 shows a general correspondence between R^* and Q_m among sites, with $R^* < Q_m$ at the clearing sites a possible consequence of additional energy contributions to melt provided by turbulent exchanges (Ellis et al., 2010). At all sites, R^* is positive over the melt period with the exception of the hypothetical NPC site where longwave losses exceed shortwave gains, resulting in a slightly negative R^* balance. Apparent in Figure 6 are the distinct differences in radiation balances between forest and clearing sites, with large shortwave gains and longwave losses at the clearing sites compared to the relatively small forest radiation balances. Marked differences are also seen in the shortwave and longwave contributions to R^* between the pine and spruce forests, with more shortwave dominated radiation at the pine forests and more longwave dominated radiation at the spruce forests.

Figure 4 inserted here

Figure 5 inserted here

Figure 6 inserted here

Discussion & Conclusions

The above results illustrate the strong control that both slope and aspect as well as forest cover have on the amounts of radiation to snow and the timing of snowmelt in Canadian

Rockies mountain environments. At these latitudes during spring, topographical self-shading of north-facing slopes contribute to producing substantial differences in shortwave irradiance between opposing open south-facing and north-facing landscapes. By contrast, shortwave differences from slope and aspect effects are much reduced under forest cover, especially in the spruce forests where the high shortwave extinction by the dense canopy cover resulted in only small shortwave contributions toward net radiation to snow and melt energy. As a result, longwave fluxes dominated radiation to snow in the spruce forests, and represented the main energy source for snowpack warming and melt. Longwave gains to spruce snowcovers were particularly pronounced during periods of above-freezing air and canopy temperatures, being large enough to facilitate rapid snowmelt. In contrast, shortwave fluxes dominated radiation to snow in pine forests during snowpack warming and melt, as the sparser canopy cover allowed for greater shortwave transmittance while simultaneously reducing canopy thermal emissions relative to spruce forest cover. Higher shortwave transmittance through the pine canopies also resulted in a sizeable variation in shortwave radiation to pine forest snowcovers due to slope and aspect. Although variations in pine forest shortwave may be partly attributed to the small differences in canopy coverage between sites, variations are also attributed to slope and aspect controls on above-canopy irradiance and beam extinction pathlength through sloping canopies. However, such slope and aspect controls were not observed under spruce forest cover, where they were effectively masked by the dense canopy coverage. Due to the sensitivity of sub-canopy shortwave irradiance to small variations in canopy coverage, a major limitation of the paper is its reliance on field observations, which do not allow for an exact delineation of forest cover controls from slope and aspect controls on forest shortwave radiation. Such an examination could be performed through focused modelling exercises, in which environmental factors could be controlled and shortwave irradiance across mountain landscapes could be assessed over a much wider range of

topography and forest coverages. However, models have their own shortcomings and uncertainties that were largely avoided by this field data approach.

In general, snowmelt rates were much more rapid at the spruce forest and clearings sites relative to the pine sites. This difference is largely ascribed to the elevation differences between the lower pine and higher spruce site locations. At the higher elevation spruce sites, the increased snowfall and cooler temperatures result in deep cold snowpacks of high thermal deficits. Consequently, melt of these high-elevation snowpacks occurs later in the spring, when shortwave irradiance is greater due to higher solar angles and longer days, and forest longwave emissions are larger due to warmer canopy temperatures. As a result, shortwave and longwave gains to snow would be expected to be substantially higher during these later spring melt periods, being capable of producing faster melt compared to the earlier melt periods at the lower-elevation pine sites, when potential shortwave and longwave gains to snow are less.

Observations at both pine and spruce locations show that slope and aspect may strongly influence forest cover effects on radiation to snow and snowmelt timing. On north-facing landscapes, shortwave reductions by forest shading are offset or slightly exceeded by longwave enhancements from canopy emissions, resulting in similar or greater amounts of radiation to forest snow. At the spruce sites, increased radiation to snow at the north-facing spruce forest corresponded with a sizeable advancement in the start of snowmelt relative to the nearby north-facing clearing where low shortwave gains and high longwave losses resulted in a large thermal deficit and delayed melt of the deep snowpack. By contrast, radiation to snow was less under pine and spruce forest cover on south-facing slopes compared to that in the open, as canopy shortwave reductions exceeded canopy longwave enhancements. In addition to reduced radiation, forest cover on south-facing slopes also resulted in a substantial delay in the start of snowmelt, and slower overall melt rates at both

the pine and spruce locations. Such results suggest that the snowmelt timing in similar mountain basins may be most sensitive to changes in forest cover on south-facing landscapes.

Compared to south-facing and north-facing sites, the effects of forest cover on radiation to snow and snowmelt timing were less pronounced on level topography. At the level pine sites, shortwave reductions under the forest canopy were counterbalanced by longwave emissions from the canopy, resulting in only a slightly decreased radiation and snowmelt rate under forest cover. Thus, unlike the marked effects of forest cover on radiation and snowmelt timing observed at the sloping sites, the results suggest less striking forest effects on level topography as the small decrease in radiation observed under pine forest cover would likely be eliminated or reversed with only slight increases in either snow albedo or canopy temperature over the winter. However, these results are instructive as they demonstrate how responses in snowmelt timing from forest cover changes on level topography may provide an unreliable proxy of effects on sloping topography. Instead, observations illustrate the potentially large variation in radiation to snow and snowmelt timing which may result from differing combinations of forest cover and slope and aspect, as well as changing springtime meteorological conditions. Such information is expected to be useful toward anticipating how forest cover changes across similar mountain headwater basins may impact the timing of river flows generated from spring snowmelt.

Acknowledgements

The authors would like to acknowledge financial support from the NOAA GEWEX Americas Prediction Project (GAPP project GC03-404); NSF-CBET Award No. 0854553; CFCAS IP3 Network, NSERC Alexander Graham Bell Scholarships and Michael Smith Foreign Scholarships, NSERC Discovery Grants, and the Canada Research Chairs programme. Field work assistance was provided by Michael Solohub and students of the Centre for Hydrology. Logistical assistance from the University of Calgary Biogeoscience Institute and Nakiska Ski Area are gratefully acknowledged.

References

Arp, C. D., Gooseff, M. N., Baker, M. A., and W. Wartsbaugh. 2006. Surface-water hydrodynamics and regimes of small mountain steam-lake ecosystems. *J. Hydrol*. **329**(3-4): 500-513.

Beaudry, P. G. and Golding, D. L. 1983. Snowmelt during rain on snow in coastal British Columbia. *Proc. Western Snow Conf.* 51, 55-66.

Black, T. A., Chen, J., Lee, X., and R. Sagar. 1991. Characteristics of shortwave and longwave irradiances under a Douglas-fir Forest stand. *Can. J. For. Res*. **21**: 1020-1028.

Cooper, D. J., Dickens, J., Hobbs, N. T., Christensen, L., and L. Landrum. 2006. Hydrologic, geomorphic and climactic processes controlling willow establishment in a montane ecosystem. *Hydrol. Process*. **20**: 1845-1864

Ellis, C. R., and J. W. Pomeroy. 2007. Estimating shortwave irradiance through needle-leaf forests on complex terrain. *Hydrol. Process*. 21: 2581-2593. doi: 10.1002/hyp.6794.

Ellis, C.R., Pomeroy, J.W., Brown, T., and J. MacDonald. Simulation of snow accumulation and melt in needleleaf forest environments. *Hydrology and Earth System Sciences,* accepted.

Essery RLH, Pomeroy JW, Ellis C, and T. Link. 2008. Modelling longwave radiation to snow beneath forest canopies using hemispherical photography and linear regression. *Hydrol. Process*., 22, 2788-2800. DOI: 10.1002/hyp.6630.

Frazer, G. W., Canham, C. D. and K. P. Lertzman. 2000. Gap Light Analyzer (GLA), Version 2.0. Technical Tools. *Bulletin of the Ecological Society of America*, pp. 191-197.

Gary, H. L. 1980. Patch Clearcuts to Manage Snow in Lodgepole Pine. Symposium on Watershed Management, *American Society of Civil Engineers*, New York, New York (held in Boise, Idaho, July 1980), 335-346.

Golding, D.L. and R.H. Swanson. 1978. Snow accumulation and melt in small forest openings in Alberta. *Can J For. Res*., 8: 380-388.

Grant, L., Seyfried, M., and J. McNamara. 2004. Spatial variation and temporal stability of soil water in a snow-dominated mountain catchment. *Hydrol. Process*. **18**: 3439-3511.

Gryning, S. and Batchvarova, E. 2001. Energy balance of a sparse coniferous high-latitude forest under winter conditions. *Boundary Layer Meteorology*, **99**: 465-488.

Harding, R. J. and J. W. Pomeroy. 1996. The energy balance of the winter boreal landscape. *Journal of Climate*. **9**: 2778-2787.

Jeffrey, W. W. Hydrology of Land Use, *In* section XIII of Handbook on the Principles of Hydrology (Ed. D.M. Gray) National Research Council of Canada. 1970.

Link, T. E. and D. Marks. 1999. Point simulation of seasonal snow cover dynamics beneath boreal forest canopies. *J. Geophys. Res*. **104**: 27841-27857.

Link, T. E., Marks, D., and J. Hardy. 2004. A deterministic method to characterize canopy radiative transfer properties. *Hydrol. Process*. **18**: 3583-3594.

Marks, D., Kimball, J., Tingey, D., and T. Link. 1998. The sensitivity of snowmelt processes to climate conditions and forest cover during rain-on-snow: A study of the 1996 Pacific Northwest Flood. *Hydrol. Process.*, 12: 1569-1587.

Marks, D. and A. Winstral. 2001. Comparison of snow depositions, the snowcover energy balance, and snowmelt at two sites in a semi-arid mountain basin. *Journal of Hydrometeorology*. **2**: 213-227.

Marks, D., Domingo, J., Susong, D., Link, T. and D, Garen. 1999. A spatially distributed energy balance snowmelt model for application in mountain basins *Hydrol. Process*. **13**: 1935-1959.

Melloh R., Hardy J., Davis R., and P. Robinson. 2001. Spectral albedo/reflectance of littered forest during the melt season. *Hydrol. Process*. **15**: 3409-3422. DOI: 10.1002/hyp.1043

Metcalfe, R.A. and J.M. Buttle. 1995. Controls of canopy structure on snowmelt rates in the boreal forest. 52nd Eastern Snow Conference, Toronto, Ontario, Canada

Moore, R. D. and J. D. Rowland. 1990. Evaluation of model performance when observed data are subject to error. *Physical Geography* **11(4)**: 379-392.

Oke, TR. 1987. *In* Boundary Layer Climates. Routledge: New York. 435 pp.

Omega Engineering Inc. 1994. Operator's manual: IRt/c Series 0S36, OS37, 0S38 Infrared Thermocouples.

Pomeroy, J.W., Rowlands, A. Hardy, J., Link, T., Marks, D., Essery, R., Sicart, J-E., and C. Ellis. 2008. Spatial Variability of Shortwave Irradiance for Snowmelt in Forests. *Journal of Hydrometeorology*, 9(6), 1482-1490.

Pomeroy JW, Marks D, Link T, Ellis C, Hardy J, Rowlands A, Granger R. 2009. The impact of coniferous forest temperature on incoming longwave radiation to melting snow. *Hydrol. Process.*, 23(17), 2513-2525. DOI: 10.1002/hyp.7325.

Pomeroy, J.W. and R.L.H. Essery. 2010. On the longwave radiant temperature of snow (in preparation for submission).

Reifsnyder, W.E., and H.W. Lull. 1965. Radiant energy in relation to forests. U.S. Department of Agriculture, Technical Bulletin No. 1344. 111 pp.

Sicart JE, Pomeroy JW, Essery RLH, Hardy JE, Link T, and D Marks. 2004. A sensitivity study of daytime net radiation during snowmelt to forest canopy and atmospheric conditions. *Journal of Hydrometeorology*, 5, 744-784.

Troendle, C. A. and C.F. Leaf. 1981. Effects of Timber Harvest in the Snow Zone on Volume and Timing of Water Yield. *In* Interior West Watershed Management. Cooperative Extension, Washington State University, Pullman, Washington (Symposium, Spokane, Washington, April 8-10, 1980), pp. 231-243.

Unites States Army Corps of Engineers, 1956. *Snow Hydrology*. U.S. Army Corps Eng., 437 pp.

Vaisala Inc. HMP45A and HMP45C humidity and temperature probes. Reference: A599en, 2008.

List of symbols

c_p	specific heat capacity of air [kJ kg^{-1} K^{-1}]
C	Celsius [°]
d	days [ ]
DOY	day of year [ ]
K_{in}	shortwave irradiance [MJ m^{-2}]
K_o	above-canopy shortwave irradiance [MJ m^{-2}]
K_{out}	reflected shortwave irradiance [MJ m^{-2}]
K^*	net shortwave radiation [MJ m^{-2}]
LAI`	effective leaf area index [m^2 m^{-2}]
L_{in}	longwave irradiance [MJ m^{-2}]
L_{out}	longwave exitance [MJ m^{-2}]
L^*	net longwave radiation [MJ m^{-2}]
LPC	level pine clearing study site [ ]
LPF	level pine forest study site [ ]
LSC	level spruce clearing study site [ ]
M	snowmelt [kg m^{-2} or mm SWE]
MB	mean bias index [ ]
MJ	mega Joules [$1e^6$ Joules]
n	count [ ]
NPC	north-facing pine clearing study site [ ]
NPF	north-facing pine forest study site [ ]
NSC	north-facing spruce clearing study site [ ]
NSF	north-sloping spruce forest study site [ ]
R^*	net all-wave radiation [MJ m^{-2}]

R^2	correlation coefficient []
SPC	southeast-facing pine clearing study site [ ]
SPF	southeast-facing pine forest study site [ ]
SSC	southeast-facing spruce clearing study site [ ]
SSF	southeast-facing spruce forest study site [ ]
SWE	snow water equivalent [kg m^{-2} or mm]
T_a	air temperature [°C or K]
T_s	snow surface temperature [°C or K]
α_s	snow albedo [ ]
β	fraction of ice in snow [ ]
Δ	slope of saturation vapour pressure curve [kPa K^{-1}]
ε_s	thermal emissivity of snow [ ]
λ_f	latent heat of fusion [MJ kg^{-1}]
λ_s	latent heat of sublimation [MJ kg^{-1}]
v	sky view factor [ ]
ρ_a	density of air [kg m^{-3}]
$\sum$	summation notation [ ]
σ	Stephan-Boltzmann constant [5.67 x 10^{-8} W m^{-2} K^{-4}]
τ	forest shortwave transmittance [ ]
ω_a	specific mixing ratio of air []
ω_s	saturation mixing ratio of air []

Ellis, CR, Pomeroy, JW, Essery, RLH & Link, TE 2011, 'Effects of needleleaf forest cover on radiation and snowmelt dynamics in the Canadian Rocky Mountains' *Canadian journal of forest research-revue canadienne de recherche forestiere*, vol 41, no. 3, pp. 608-620.

Table 1. Topographic and forest cover descriptions of pine and spruce study sites.

Site:	*Elevation* [m.a.s.l.]	*Slope gradient* [°]	*Slope aspect* [°]	*Forest coverage*	*number of hemispherical images/LAI` measures*	*Mean LAI`*	*LAI`* (standard deviation)	*Sky view factor* (*v*)
Level pine clearing site (LPC)	1457	0	-	none	1	0†	-	0.96
Level pine forest site (LPF)	1492	0	-	continuous	46	1.48	0.21	0.22
North-facing pine forest site (NPF)	1480	29	351	continuous	32	1.57	0.10	0.19
North-facing pine clearing site (NPC)*	1480	29	351	none	-	0*	-	0.96
Southeast-facing pine clearing sites (SPC)	1526	27	128	none	1	0†	-	0.93
Southeast-facing pine forest site (SPF)	1523	26	125	discontinuous	57	1.33	0.32	0.34
Level spruce clearing site (LSC)	1848	0	-	none	1	0†	-	0.96
North-facing spruce clearing site (NSC)	2040	29	347	none	1	0†	-	0.95
North-facing spruce forest site (NSF)	2037	28	348	continuous	26	1.8	0.11	0.16
South-facing spruce clearing site (SSC)	2012	27	176	continuous	1	0†	-	0.95
South-facing spruce forest site (SSF)	2008	28	176	none	21	2.4	0.13	0.09

*hypothetical site assigned the same slope and aspect as the NPF and the same sky view factor (*v*) as the LPC.

†value refers to the centre of the clearing and does not include surrounding vegetation.

Table 2. Summary of the mean meteorological conditions observed at the 2005 pine and 2008 spruce level clearing sites over the extended observation period and the period of snowpack warming and melt.

Site	*Period*	*Shortwave irradiance* (K_{in})	*Longwave irradiance* (L_{in})	*Relative humidity*	*Air temperature* (T_a)
units		[MJ m^{-2}]	[MJ m^{-2}]	[%]	[°C]
Level Pine Clearing (LPC)	Extended observation period (DOY 46-135, 2005)	13.2	22.0	62	2.4
Level Pine Clearing (LPC)	Period of snowpack warming and melt (DOY 72-95, 2005)	12.1	22.6	60	0.9
Level Spruce Clearing (LSC)	Extended observation period (DOY 46-136, 2008)	14.5	20.5	66.2	-1.3
Level Spruce Clearing (LSC)	Period of snowpack warmer and melt (DOY 90-150, 2008)	15.1	19.8	63.4	-3.4

Table 3. Specifications and accuracy of the shortwave (K) and longwave (L) radiometers used for field observations.

Sensor model	*Site*	*Measured flux*	*Number of sensors at site*	*Sensor class‡*	*Spectral range*	*Expected accuracy for daily totals†*
Kipp & Zonen CM-3 pyranometer	LPC, LPF, NPF, SPC, SPF, NSF, SSF	K_{in}, K_{out}	2	2	305-2800 nm	±10%
Kipp & Zonen CG-3 pyrgeometer	LPC, LPF, NPF, SSC, SPF, NPF, SSF	L_{in}, L_{out}	2	2	5-50 μm	±10%
Kipp & Zonen CM-5 pyranometer	SPF	K_{in}	2	2	300-2800 nm	±10%
Kipp & Zonen CG-1 pyrgeometer	SPF, LSC	L_{in}	2	2	5-42 μm	±10%
Kipp & Zonen CM-21 pyranometer	SPC, LSC	K_{in}	1	1	305-2800 nm	±2%

* as specified by the International Organization for Standardization (ISO).

†as specified by the radiometer manufacturer.

Table 4. Mean bias (*MB*) of daily shortwave irradiance (K_{in}) and longwave irradiance (L_{in}) observed by the permanent *site* radiometers at the level pine forest (LPF) and the southeast-sloping pine (SPF) sites as calculated relative to irradiance observed by a multi-sensor radiometer *array*.

DOY:	*67*	*68*	*69*	*70*	*71*	*72*	*73*	*74*	*75*	*76*	***Overall Mean Bias Index (MB)***	*Mean daily irradiance (array)* [MJ m^{-2}]	*Mean daily irradiance (site)* [MJ m^{-2}]	*array-site irradiance* [MJ m^{-2}]
K_{in} MB (SPF)	0.99	0.98	0.98	0.96	0.95	0.98	0.97	-	-	-	**0.98**	4.56	4.70	0.14
L_{in} MB (SPF)	1.03	1.03	1.06	1.07	1.06	1.03	1.03	-	-	-	**1.04**	25.2	24.2	1.00
K_{in} MB (LPF)	-	-	-	-	-	-	-	0.99	0.99	0.99	**0.99**	2.50	2.47	0.03
L_{in} MB (LPF)	-	-	-	-	-	-	-	1.00	1.02	1.00	**1.01**	24.9	24.7	0.20

Table 5. Mean daily shortwave irradiance (K_{in}) at each study site over the extended observation period of February 15 to May 15 stated in terms of mean irradiance and the ratio relative to the respective level clearing site (*). For the forest sites, the mean shortwave transmittance of forest cover (τ) is also given.

Site	Mean daily K_{in} [MJ m^{-2}]	Ratio to level clearing site []	Forest shortwave transmittance (τ) []
*LPC	13.2	1	-
LPF	2.9	0.22	0.22
NPC	10.5	0.80	-
NPF	1.4	0.11	0.13
SPC	15.8	1.20	-
SPF	5.4	0.41	0.34
*LSC	14.5	1	-
NSC	11.8	0.81	-
NSF	1.5	0.10	0.12
SSC	16.4	1.13	-
SSF	1.7	0.12	0.11

Table 6. Mean longwave irradiance (L_{in}) at each study site for the extended observation period of February 15 to May 15 stated in terms of mean irradiance and the ratio relative to the respective level clearing site (*).

	Longwave irradiance (L_{in})		
Site	Mean daily L_{in} [MJ m^{-2} d^{-1}]	Ratio to level clearing site []	Difference to level clearing site [MJ m^{-2} d^{-1}]
*LPC	22.0	1.0	0.0
LPF	25.9	1.17	3.9
NPC	22.0	1.0	0.0
NPF	26.1	1.18	4.1
SPC	22.2	1.01	0.2
SPF	26.6	1.21	4.6
*LSC	19.8	1.0	0.0
NSC	19.8	1.0	0.0
NSF	24.2	1.22	4.4
SSC	19.8	1.0	0.0
SSF	24.4	1.23	4.6

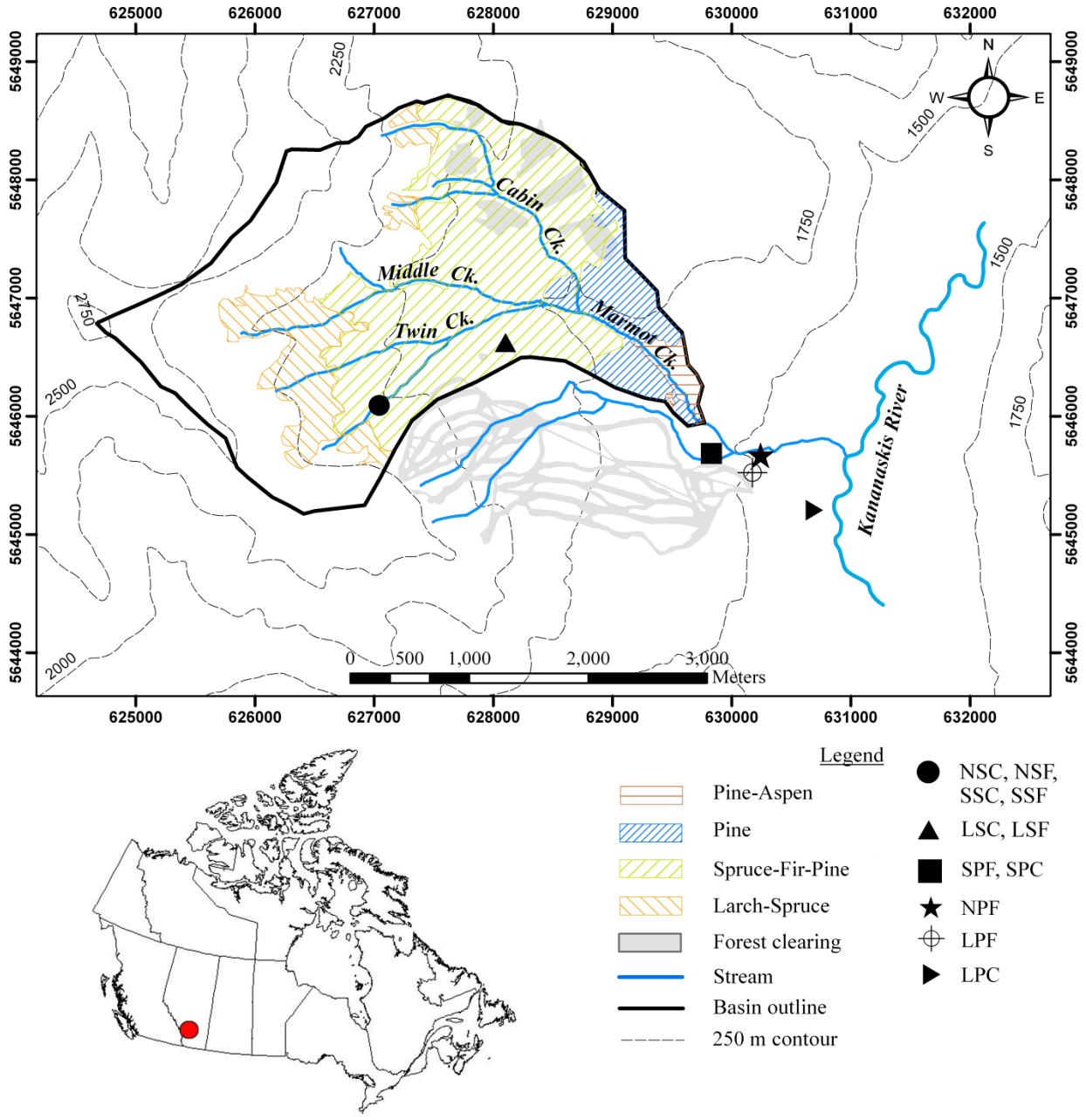

Figure 1. Top: Map of the Marmot Creek Research Basin (MCRB) showing the locations of the level pine clearing (LPC), level forest pine forest (LPF), north-sloping pine clearing (NPC), north-sloping pine forest (NPF), southeast-sloping pine clearing (SPC), southeast-sloping pine forest (SPF), level spruce clearing (LSC), north-sloping spruce forest (NSF), south-sloping spruce forest (SSF), north-sloping spruce clearing (NSC), and south-sloping spruce clearing (SSC) sites. Inset indicates the general location of the MCRB.

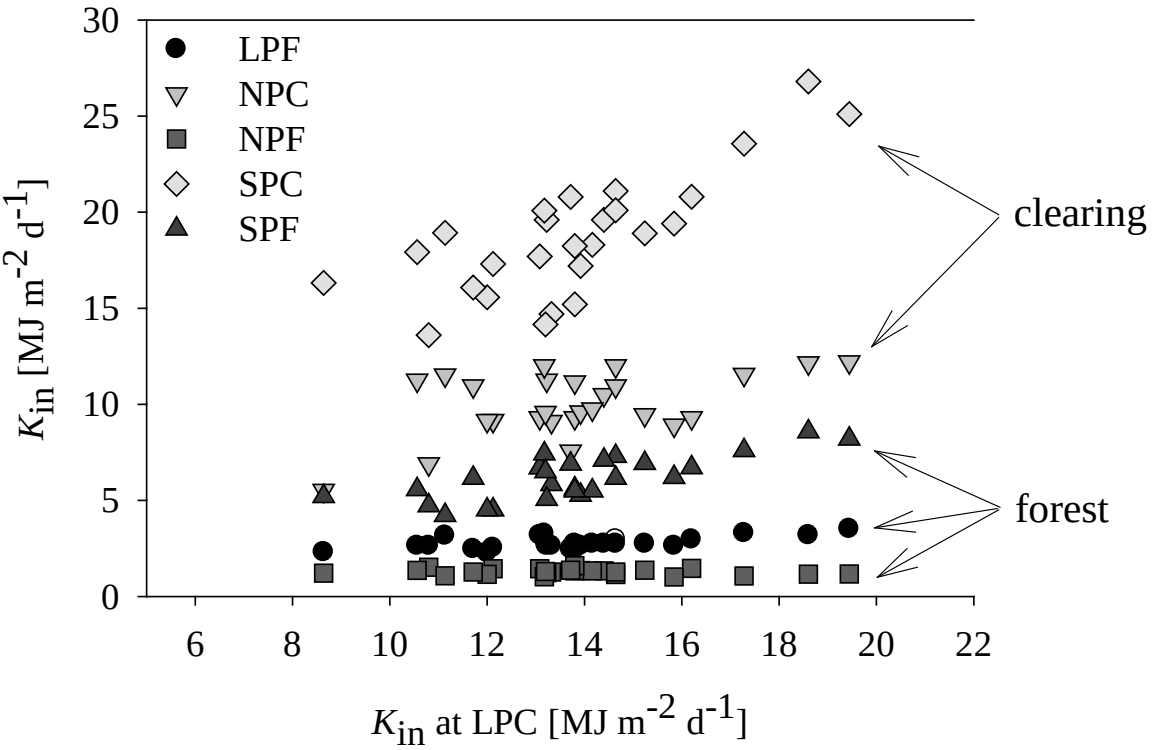

Figure 2. Relation between the daily shortwave irradiance (K_{in}) observed at the level pine clearing site (LPC) compared to K_{in} observed at the level pine forest site (LPF), southeast-facing pine clearing site (SPC), the southeast-facing pine forest site (SPF), the north-facing pine forest site (NPF), and simulated at the north-facing pine clearing site (NPC) for the period of April 3 to April 29, 2005.

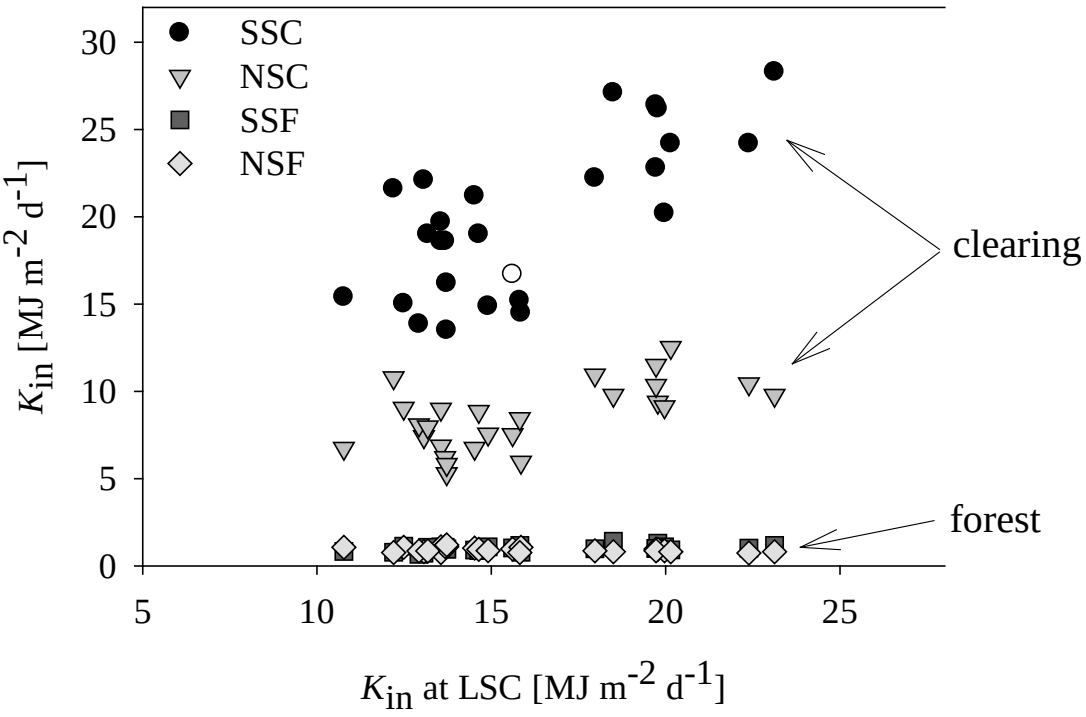

Figure 3. Relation between the daily shortwave irradiance (K_{in}) observed at the level spruce clearing (LSC) site compared to K_{in} observed at the north-facing spruce forest (NSF) and south-facing spruce forest (SSF) sites, and simulated K_{in} at the north-facing spruce clearing (NSC) and south-facing spruce clearing (SSC) sites for the period of April 3 to April 29, 2008.

(a)

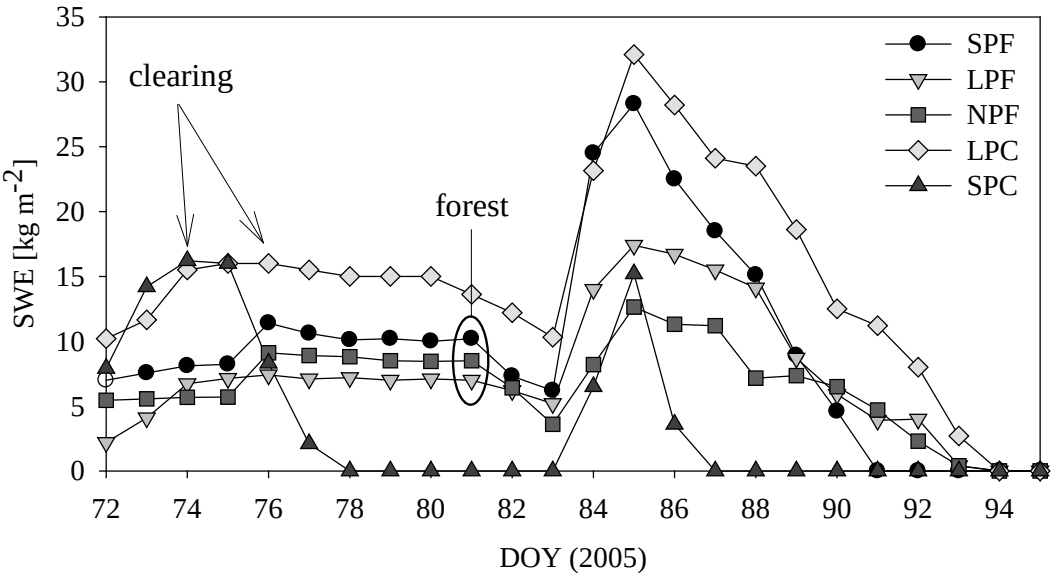
clearing
forest
SPF
LPF
NPF
LPC
SPC
SWE [kg m-2]
DOY (2005)

(b)

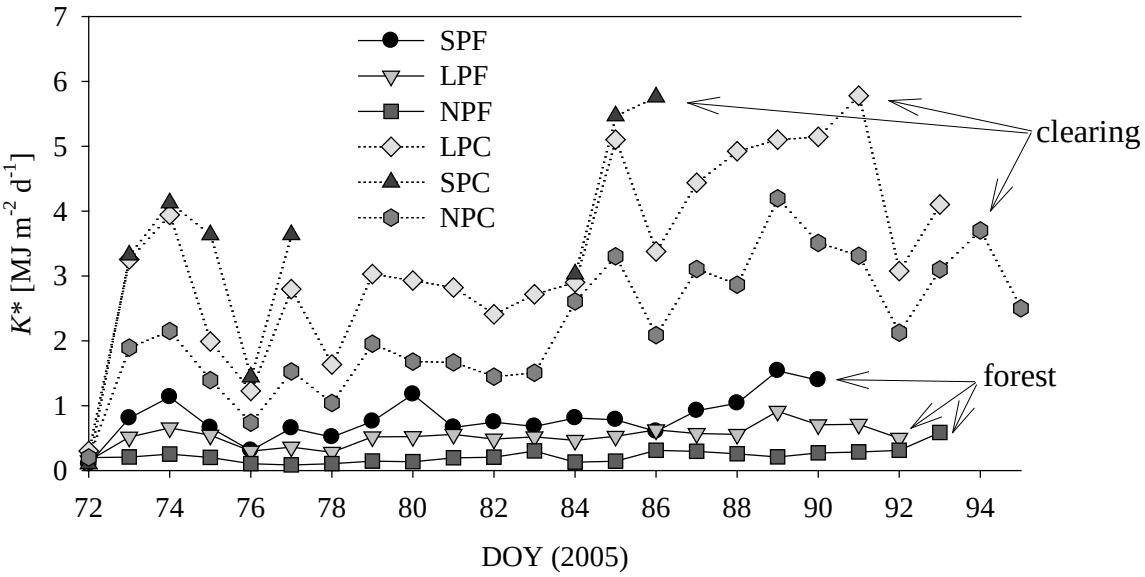
SPF
LPF
NPF
LPC
SPC
NPC
clearing
forest
K* [MJ m-2 d-1]
DOY (2005)

(c)

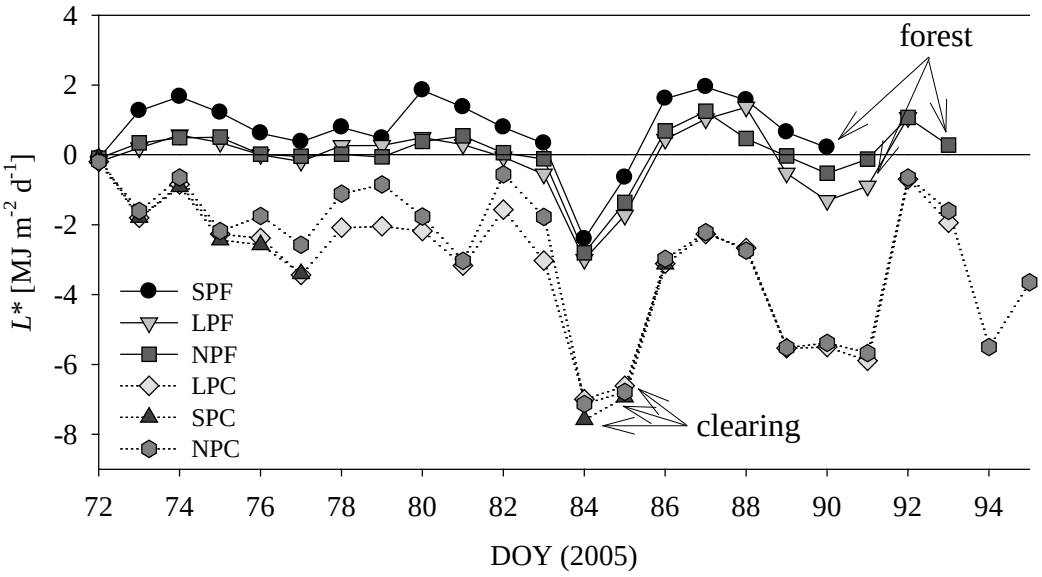

Figure 4. Time series plots at the pine sites during the 2005 period of snowpack warming and melt showing: (a) snow water equivalent (SWE), (b) daily net shortwave radiation to snow (*K**), and (c) daily net longwave radiation to snow (*L**).

(a)

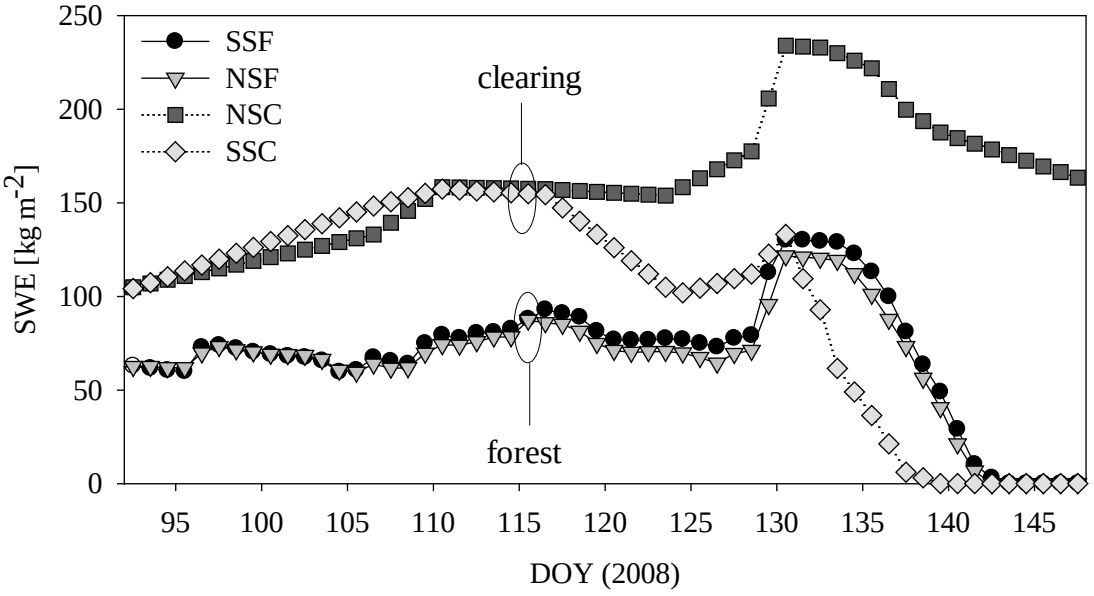
SSF
NSF
NSC
SSC
clearing
forest
SWE [kg m-2]
DOY (2008)

(b)

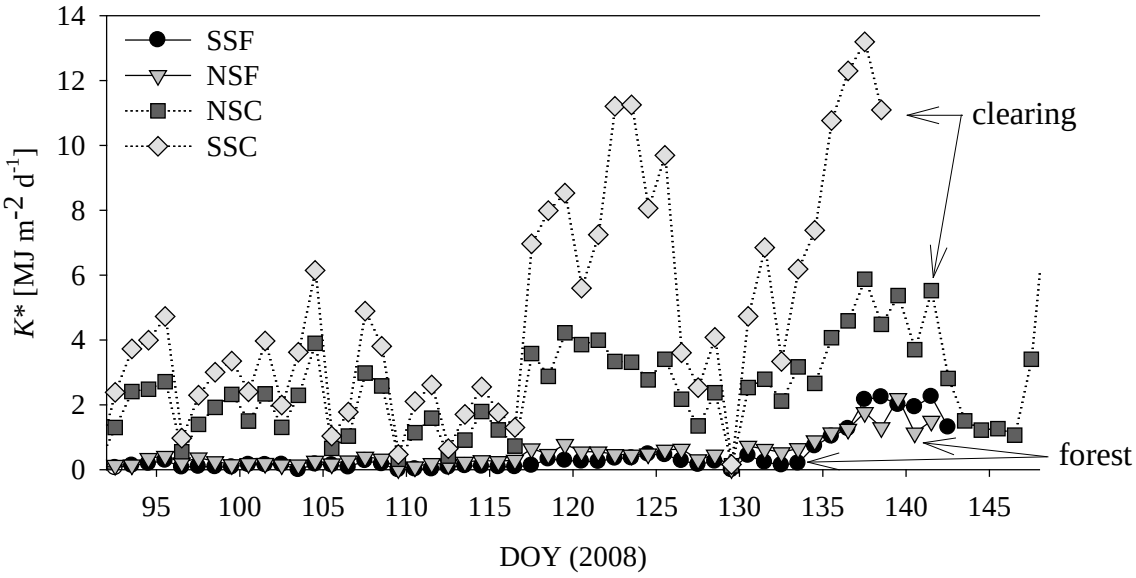
SSF
NSF
NSC
SSC
clearing
forest
K* [MJ m-2 d-1]
DOY (2008)

(c)

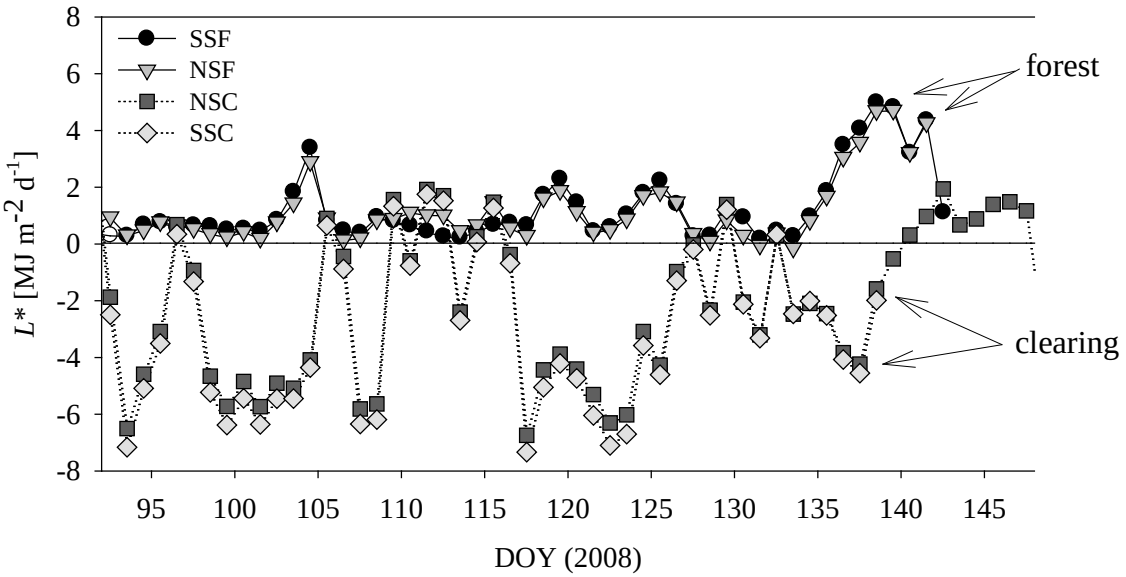

Figure 5. Time series plots at the spruce sites during the 2008 period of snowpack warming and melt showing: (a) snow water equivalent (SWE), (b) daily net shortwave radiation to snow (*K**), and (c) daily net longwave radiation to snow (*L**).

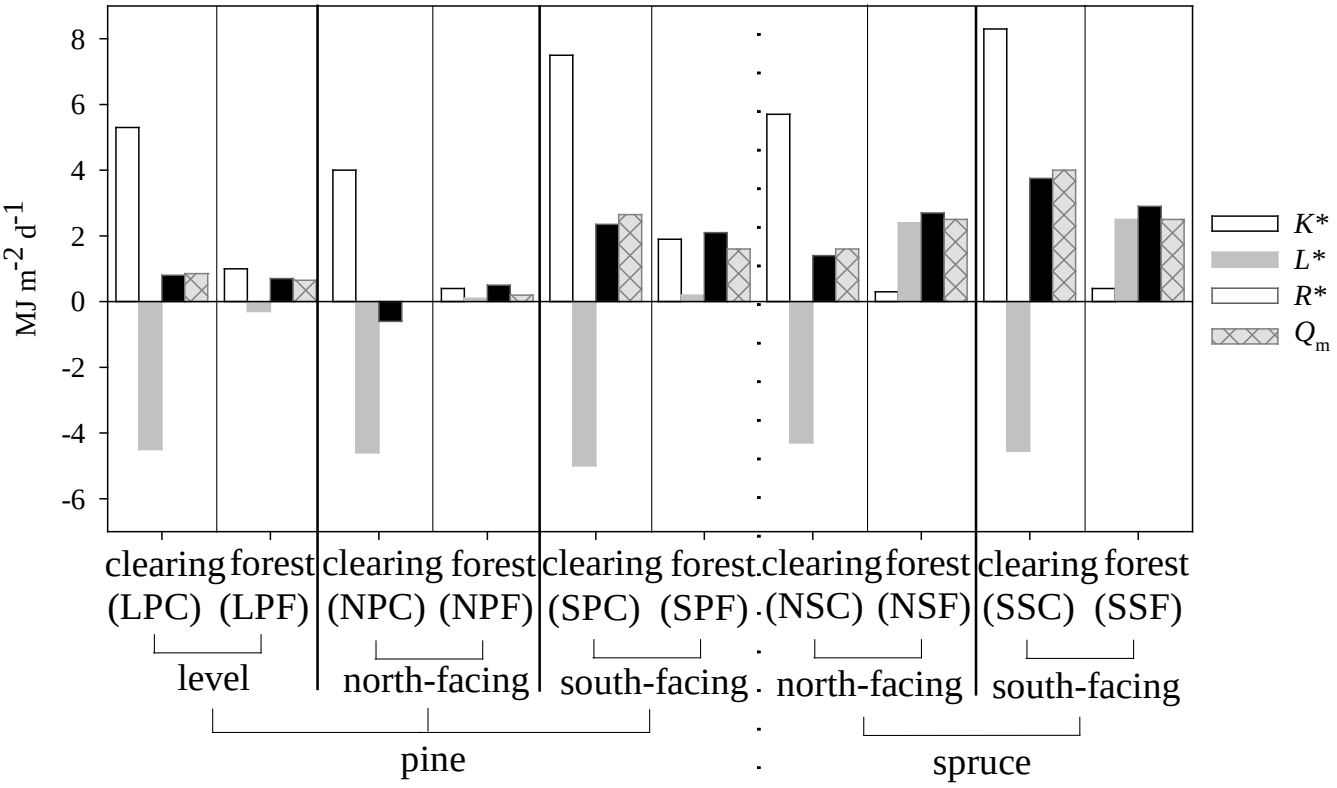

Figure 6. Mean daily net shortwave radiation (K^*), net longwave radiation (L^*), net all-wave radiation (R^*), and snowmelt energy (Q_m) during the main snowmelt event at the pine study sites (starting DOY 84) and the spruce study sites (starting DOY 130).